

MSCoTDet: Language-driven Multi-modal Fusion for Improved Multispectral Pedestrian Detection

Taeheon Kim*, Sangyun Chung*, Damin Yeom, Youngjoon Yu, Hak Gu Kim and Yong Man Ro, *Senior Member, IEEE*.

Abstract—Multispectral pedestrian detection is attractive for around-the-clock applications due to the complementary information between RGB and thermal modalities. However, current models often fail to detect pedestrians in certain cases (e.g., thermal-obscured pedestrians), particularly due to the modality bias learned from statistically biased datasets. In this paper, we investigate how to mitigate modality bias in multispectral pedestrian detection using Large Language Models (LLMs). Accordingly, we design a Multispectral Chain-of-Thought (MSCoT) prompting strategy, which prompts the LLM to perform multispectral pedestrian detection. Moreover, we propose a novel Multispectral Chain-of-Thought Detection (MSCoTDet) framework that integrates MSCoT prompting into multispectral pedestrian detection. To this end, we design a Language-driven Multi-modal Fusion (LMF) strategy that enables fusing the outputs of MSCoT prompting with the detection results of vision-based multispectral pedestrian detection models. Extensive experiments validate that MSCoTDet effectively mitigates modality biases and improves multispectral pedestrian detection.

Index Terms—Multispectral Chain-of-Thought Detection, Language-driven Multi-modal Fusion, Multispectral Pedestrian Detection, Large Language Models.

I. INTRODUCTION

Multispectral pedestrian detection is the task of detecting pedestrians based on different visual modalities (i.e., RGB and thermal) [1]–[9]. Due to their complementary information, combining these modalities improves pedestrian detection all day/night [10]–[13]. With advances in this field, the primary interest in multispectral pedestrian detection has been focused on effectively fusing the complementary information between the two modalities. Previous works investigated various fusion methods in different stages of the network, which are often categorized as early-fusion [14], mid-fusion [15]–[17], and late-fusion [14], [18]. These methods demonstrated superior detection performance compared to standard pedestrian detection [19]–[29], especially in practical datasets [11], [30], [31] that contain all day/night scenarios.

Despite the progress in this task, there are still remaining

problems that need to be solved. From a recent work [16], multispectral pedestrian detection models are known to rely on spurious modality bias toward the thermal modality, due to learning the statistical bias in datasets. In multispectral pedestrian datasets, the pedestrian always statistically co-occur with its thermal signatures [16] because the thermal modality is generally robust both day/night (Fig. 1 (a)). Models trained on these datasets learn the statistical co-occurrences of thermal signatures associated with pedestrians. As a result, models often fail on test data in which such co-occurrences do not hold, e.g., pedestrians with obscured thermal signatures (or, *thermal-obscured* pedestrians). In the real world, thermal-obscured pedestrians are captured when intermediate obstacles, such as heat-insulating cloth or glass windows, block thermal radiation from reaching the thermal camera. Fig. 1 (b) demonstrates a multispectral pedestrian detector predicts the thermal-obscured pedestrian based on its absence of thermal signature, leading to failed detections. Such a phenomenon implies that modality biases limit the generalization of multispectral pedestrian detection models.

In this paper, we aim to address the aforementioned problems. Developing a model that performs unbiased inference is challenging from biased training. This challenge arises due to a lack of explicit visual priors in training data. While increasing supervision of these priors through extra annotations or data augmentation could be one solution, it is difficult to achieve. It is because detection failures due to modality biases are not just limited to specific cases, such as thermal-obscured pedestrians, but are common in real-world data. For example, models often mistakenly detect trees or fireplugs as pedestrians due to their similar thermal signatures. It is difficult to find all detection failure cases caused by modality biases and augment the training priors accordingly [16], [32]. And the cost of multispectral data collection and manual annotation is prohibitive [18].

However, such priors may be obtained from a large language model, well-known for its wide encapsulation of knowledge and generalization ability. Thus, we investigate the approach of leveraging large language models (LLMs) [33]–[38] in addressing modality biases without additional data supervision. LLMs can understand the scene or context detailed in the text and apply their common-sense knowledge to connect visual information across different modalities [39]. Based on this ability, an LLM can determine which modality of information should be referred to more and intervene in modality biases. An example is illustrated in Fig. 1 (c). An LLM understands that a person wearing heat-insulation clothing is invisible

*: Both authors contributed equally to this manuscript.

This work was conducted by Center for Applied Research in Artificial Intelligence (CARAI) grant funded by DAPA and ADD (UD230017TD) (Corresponding author: Yong Man Ro).

T. Kim, S. Chung, D. Yeom, Y. Yu, and Y. M. Ro are with Integrated Vision and Language Lab., School of Electrical Engineering, Korea Advanced Institute of Science and Technology (KAIST), 291 Daehak-ro, Yuseong-gu, Daejeon, 34141, Republic of Korea (e-mail: eetaekim@kaist.ac.kr; jellarum@kaist.ac.kr; damin321@kaist.ac.kr; great-day@kaist.ac.kr; ymro@kaist.ac.kr).

H.G. Kim is with Department of Image Science and Arts, GSAIM, Chung-Ang University, Seoul, 06974, Republic of Korea (e-mail: hakgukim@cau.ac.kr).

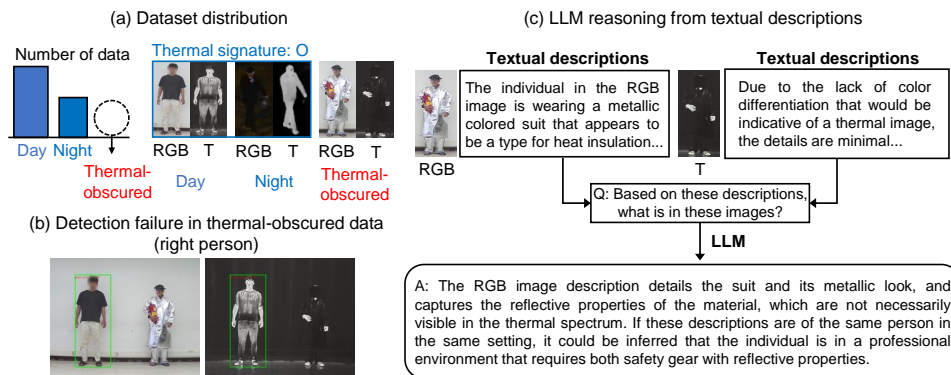


Fig. 1. Problem illustration and our motivation. (a) In multispectral pedestrian datasets, thermal signatures always appear on pedestrians, as the thermal modality can generally capture pedestrians all day/night. In these datasets, thermal-obscured data is underrepresented. Models trained on such datasets learn the statistical co-occurrences between pedestrians and their thermal signatures. (b) As a result, models fail to detect pedestrians in thermal-obscured data, even though obviously visible in RGB. (c) An example of prompting the LLM. Based on the textual descriptions of RGB and thermal images, we prompt the ChatGPT [40] to answer the question “Based on these descriptions, what is in these images?”. The ChatGPT detects the person without suffering modality biases, realizing that a person wearing heat-insulation clothing is invisible in thermal images due to the reflective material. Our motivation is to develop MSCoT prompting based on LLMs and integrate it into vision-based multispectral pedestrian detectors.

in thermal images due to the reflective material. From such understanding, the LLM relies on the RGB information for predicting the pedestrian.

Based on our preliminary findings, we design the Multispectral Chain-of-Thought (MSCoT) prompting, which prompts the LLM to perform the task of multispectral pedestrian detection. For the inputs of MSCoT prompting, we obtain textual descriptions of pedestrians in both RGB and thermal images from a pre-trained multi-modal language model (MLLMs) [41]. Our goal of MSCoT prompting is to produce probabilistic detection scores from these textual descriptions. However, LLMs are known for their overconfidence [42]–[44] and output confidence scores irrelevant to the context [45]. To overcome this problem, we designed MSCoT prompting to conduct two consecutive Chain-of-Thought [46] (CoT) prompting steps. MSCoT prompting first outputs uni-modal confidence scores and comprehends them with the text of both modalities to produce final detection scores. From these processes, MSCoT prompting facilitates LLMs to produce reliable detection scores that are compatible with multispectral pedestrian detectors.

Building on our MSCoT prompting, we propose the MSCoTDet framework that produces unbiased detections from a statistically biased train set. This problem formulation is adopted rather than explicitly modifying the training priors (such as adding thermal-obscured pedestrians in the train set) to verify that MSCoT prompting can effectively intervene in the modality bias of multispectral pedestrian detectors. Specifically, the MSCoTDet framework integrates the decision processes of MSCoT prompting into vision-based multispectral pedestrian detectors. A Language-driven Multi-modal Fusion (LMF) is designed to effectively integrate these two distinct decision processes.

To evaluate the effectiveness of MSCoTDet, we conduct experiments on generic multispectral pedestrian datasets (FLIR [30], and CVC-14 [31]) and a dataset (ROTX-MP [16]) that mainly contains thermal-obscured pedestrians. Extensive experiment results show that MSCoTDet generalizes well on ROTX-MP even with biased training data while performing

robustly on generic datasets.

Contributions. In summary, our contributions are:

- 1) We propose the Multispectral Chain-of-Thought (MSCoT) prompting strategy, which prompts the LLM to perform the task of multispectral pedestrian detection.
- 2) We propose the MSCoTDet framework, which integrates MSCoT prompting into vision-based multispectral pedestrian detectors.
- 3) Extensive experiments demonstrate that our proposed MSCoTDet framework can significantly intervene in modality bias and improve the overall performance of multispectral pedestrian detectors.

II. RELATED WORK

A. Multispectral Pedestrian Detection

Dataset. Different from standard pedestrian detection [47]–[53], multispectral pedestrian detection aims to detect pedestrians using RGB and thermal images. One challenge in multispectral pedestrian detection is the lack of data. The process of aligning RGB and thermal images requires expensive hardware, such as a beam-splitter [11] and a GPS clock. For annotating bounding boxes of multispectral data, each modality needs separate annotations.

The KAIST [11] dataset is one of the first benchmarks for multispectral pedestrian detection, containing well-aligned RGB and thermal images. The FLIR [30] data offers higher image resolution than KAIST [11]. On the other hand, the CVC-14 [31] dataset largely contains misaligned RGB-thermal images. ROTX-MP [16] dataset highlights the challenge due to the dataset bias of multispectral data. ROTX-MP adopts the evaluation setting where the test distribution is significantly different from the training priors. Performing unbiased inference with biased training data remains a challenge in multispectral pedestrian detection.

Models. Previous studies focused on developing various fusion methods for multispectral pedestrian detection. These approaches are based on early-fusion, mid-fusion, or late-fusion, which are often categorized by the fusion stage of the network. Specifically, early-fusion [14] methods concatenate RGB and

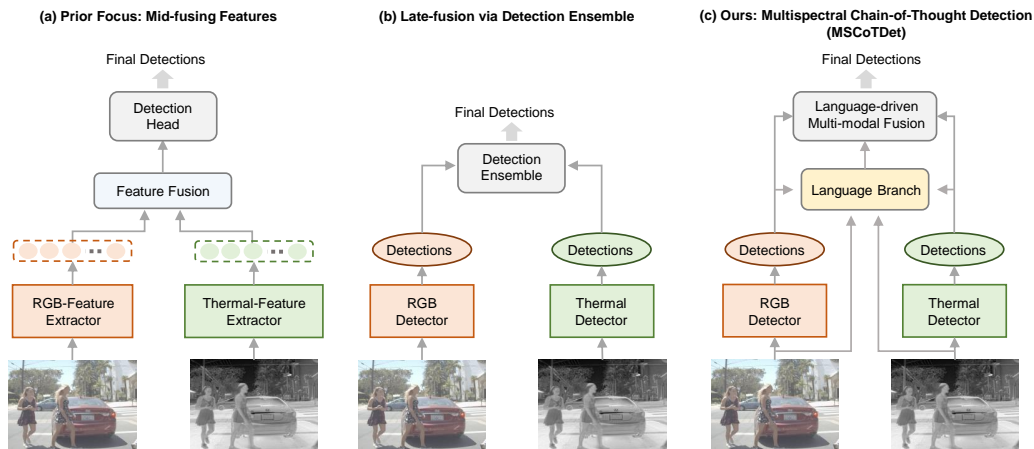


Fig. 2. Comparisons between previous works and our method (MSCoTDet). (a) Previous approaches centrally focused on mid-fusion methods, e.g., mid-fusing features internally in the network. (b) There are few works via late fusion that ensemble detections from independently trained single-modal detectors, i.e., RGB and thermal detectors. (c) MSCoTDet (Ours) focuses on designing a language branch that processes detection using Large Language Models (LLMs). The language branch includes the MSCoT prompting, which prompts the LLM to perform multispectral pedestrian detection. Then, our proposed Language-driven Multi-modal Fusion (LMF) enables fusing vision-driven and language-driven detections.

thermal images at the input stage and processes through the detection network. Mid-fusion [5], [10], [14], [54] has been the prior focus, which encodes RGB images and thermal images to the same feature space and fuses them inside the network. However, early-fusion and mid-fusion are known to memorize the training priors and exhibit poor generalizability [16] on out-of-distribution data. Lastly, late-fusion [18], [55] methods are based on ensembling detection results produced from RGB and thermal single-modal detectors. Most of them do heuristic weighting with single-modal detectors or perform simple Bayesian estimation, leading to reduced accuracy. In this work, our MSCoTDet framework prompts large language models (LLMs) to perform multispectral pedestrian detection. This approach enables two key advancements: 1) the fusion of multimodal data based on a semantic understanding of the multimodal (inter-modality) context, and 2) the adoption of large language models’ (LLMs) generalization capability.

B. Addressing Modality Biases in Multimodal Learning

As modality biases significantly influence the reliability of multi-modal models, several endeavors have been devoted to solving modality bias issues in different multi-modal tasks such as classification [56], visual question answering (VQA) [32], and person re-identification [57]. One straightforward approach to mitigate modality bias is to augment the training data or use additional annotations. In particular, counterfactual generation [58]–[61] helps to balance the training data by explicitly adding the out-of-distribution priors. However, in the real world, unknown test cases are prevalent, and augmenting all these cases is difficult due to the vast diversity of real-world data [16], [32]. Therefore, various benchmarks (e.g., VQA-CP [62], ROTX-MP [16]) were proposed to evaluate whether multimodal models generalize well in subtly different distributions from training data.

Under these benchmarks, Wang et al. [56] proposed Gradient Blending, which combines gradient estimates by calculating optimal weights for each modality. Gat et al. [63] leverages the log-Sobolev inequality to bound the functional entropy,

effectively maximizing the utilization of each modality’s information during training. Niu et al. [32] capture the language bias in the VQA task as the natural direct effect of questions on answers. The debiasing is achieved by subtracting the language bias from the total effect. Similarly, our previous work [16] aims to mitigate the thermal modality bias in multispectral pedestrian detection through counterfactual intervention. They subtract the detection score of the direct thermal path from the total detection score. Different from them, our MSCoTDet is designed to fuse modalities based on realizing the semantic context between the multimodal inputs and outputs. MSCoTDet output predictions based on the encapsulation of task knowledge by utilizing an LLM, which can be equally applied to make robust decisions when inferring out-of-distribution data.

C. Vision Tasks with LLMs

Large language models (LLMs) excel in natural language processing (NLP) and generation by training on vast amounts of text data [33]–[38]. These features and advantages offer innovative applicability across more general areas of intelligence, such as computer vision. Yang et al. [64] introduced LLM-guided concept bottlenecks (LaBo) for image classification. LaBo generates candidate concepts from GPT-3 [34] and align them to test images by computing similarity scores. Naeem et al. [65] enhance zero-shot image classification framework utilizing an LLM to create web-scale documents. They compute the multiple complementary views of each class between text and image features and perform image classification. Khan et al. [66] improve VQA models by annotating unlabeled images with an LLM. Park et al. [24] proposed a pedestrian detection framework that integrates LLM-derived text features via clustering and task-prompting. They create a document of pedestrian appearance descriptions using an LLM and combine them with visual features inside the pedestrian detection network. The majority of approaches that leverage LLM on vision tasks often 1) create large documents with LLMs [24], [34], [65], 2) combine or compare text and

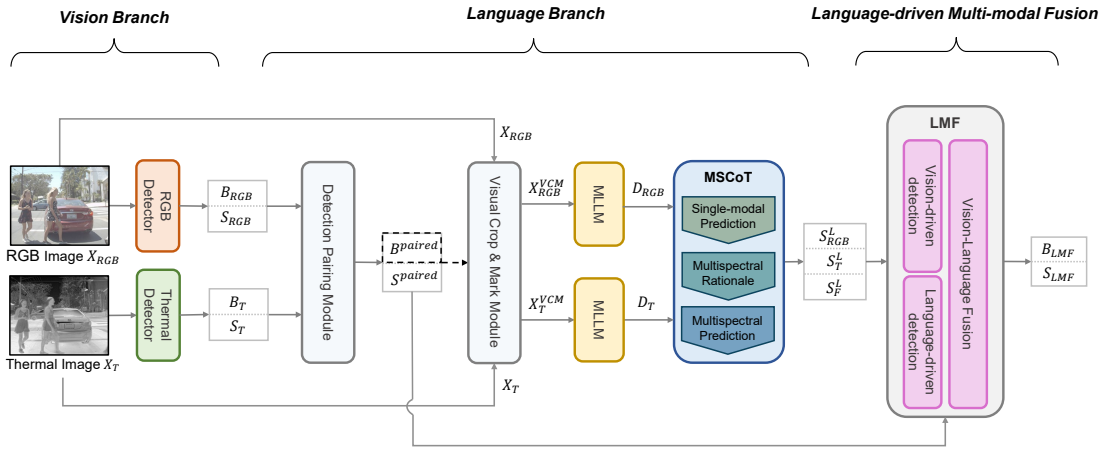


Fig. 3. Overall architecture of proposed Multispectral Chain-of-Thought detection (MSCoTDet) framework including vision branch, language branch, and language-driven multi-modal fusion.

image features internally in the network [24], [34], [65], or 3) augment training data [66]. Different from previous works, we focus on prompting the LLM to perform the vision task (i.e., multispectral pedestrian detection) so that it fully exploits its linguistic capabilities. Furthermore, our proposed method completely sidesteps the need for constructing large documents or collecting/augmenting additional data.

III. PRELIMINARIES

Before introducing our method, we review the late-fusion strategies in multispectral pedestrian detection. Then we elaborate on our proposed method.

A. Late-fusion in Multispectral Pedestrian Detection

Rather than fusing modalities in the input stage (early-fusion [67]–[69]) or in the intermediate steps (mid-fusion [10], [17]), late-fusion [18], [70] is based on detection ensembling, i.e., fusing the decision values. One of the advantages of late fusion is that it can preserve single-modal models and, therefore, has high flexibility to perform multi-modal fusion from diverse models of different modalities [70]–[75], e.g., *fusing predictions between LLMs and vision-based detectors*. Late fusion methods have been also investigated in multispectral pedestrian detection [18]. They first train single-modal detectors (i.e., RGB and thermal) and then fuse the prediction scores (score fusion) and bounding boxes (box fusion) which are the outputs from single-modal detectors. The final output includes fused prediction scores and bounding boxes. We describe score fusion and box fusion strategies below.

Score Fusion. The most common strategies to fuse prediction scores obtained from single-modal models are averaging [5], [6], Non-maximum Suppression (NMS) [18], and Probabilistic Ensembling (ProbEn [18]). Between them, we adopt averaging and NMS, as we find them effective for our method (Section IV-D). Averaging is straightforward, the fused score is determined by averaging prediction scores estimated in each modality. Denote s_{RGB} and s_T the prediction scores predicted for the same object in different modalities (i.e., RGB

and thermal). Then the averaging score fusion between s_{RGB} and s_T can be expressed as:

$$s_{AVG} = \frac{s_{RGB} + s_T}{2}, \quad (1)$$

where s_{AVG} denotes the fused score. On the other hand, NMS compares the prediction scores estimated in each modality and votes for the highest one, removing the lower scores. NMS score fusion between s_{RGB} and s_T can be expressed as:

$$s_{NMS} = \max(s_{RGB}, s_T), \quad (2)$$

where s_{NMS} denotes the fused score by the NMS.

Box Fusion. Box fusion is to merge overlapping bounding boxes predicted from different modalities (i.e., RGB and thermal). Chen et al.(2022) [18] suggests a simple and effective way to probabilistically fuse boxes, which computes a weighted average of boxes. The weights are given by the prediction scores, implying that more confident detections should have a higher weight when fusing boxes. Denote b_{RGB} and b_T the bounding box coordinates predicted for the same object in different modalities (i.e., RGB and thermal). Using the predictions scores s_{RGB} , and s_T , the weighted-averaging box fusion between b_{RGB} and b_T can be expressed as:

$$b_{s-avg} = \frac{b_{RGB} \times s_{RGB} + b_T \times s_T}{s_{RGB} + s_T}, \quad (3)$$

where b_{s-avg} denotes the fused bounding boxes.

Our Motivation. Previous works have studied late-fusion approaches in multispectral pedestrian detection with two single-modal detectors, i.e., an RGB object detector and a thermal object detector. Most do heuristic weighting with single-modal detectors or perform simple Bayesian estimation [18]. Therefore, these methods sometimes neglect the inter-modality contexts that might differ between the diverse scenarios of multispectral pedestrian detection. One advantage of late-fusion is that it preserves the single-modal predictions, as it does not require aligning different modalities in the same domain (early-fusion) or feature space (mid-fusion). Our motivation is to leverage the late-fusion strategies to fuse predictions from LLMs and vision-based detection

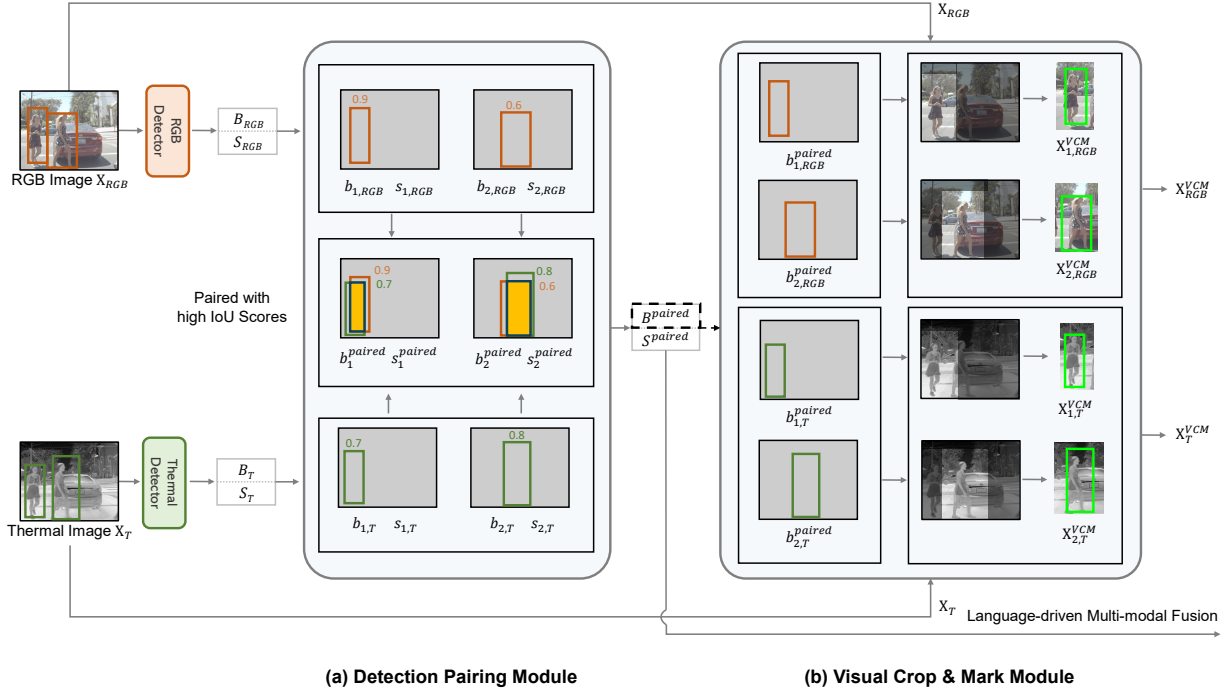


Fig. 4. Visualized details of the (a) Detection Pairing Module and the (b) Visual Crop & Mark Module. (a) The Detection Pairing Module gets single-modal detections from the vision branch and then finds the detection pairs that belong to the same pedestrians, e.g., $b_1^{paired} = (b_{1,RGB}^{paired}, b_{1,T}^{paired})$ and $s_1^{paired} = (s_{1,RGB}^{paired}, s_{1,T}^{paired})$. Through the iteration of pedestrians, the module produces the sets of paired detections B^{paired} and S^{paired} . (b) The Visual Crop & Mark Module gets B^{paired} as inputs, and output the sets of pre-processed images X_{RGB}^{VCM} and X_T^{VCM} .

models. To this end, we design the Language-driven Multi-modal Fusion (LMF) in Section IV-D. In the next section, we propose the MSCoTDet framework and describe its details.

IV. PROPOSED METHOD

A. Overall Architecture

The overall architecture of our proposed MSCoTDet framework is shown in Fig. 3. It consists of two branches that perform distinct detection processes, the vision branch and the language branch. Detections from these branches are fused to output final detections. We briefly introduce the process of each branch and our fusion strategy.

Vision branch. Given the input of RGB and thermal images X_{RGB} and X_T , the vision branch first produces single-modal (i.e., RGB or thermal) detections. Denote the prediction scores as S_{RGB} , S_T and bounding boxes as B_{RGB} , B_T produced from each single-modal detector. The single-modal detections in the vision branch are processed through the language branch.

Language Branch. The language branch first generates text descriptions of pedestrians and performs detections based on them. Toward this goal, we leverage Multi-modal Large Language Models (MLLMs), which are capable of generating comprehensive descriptions in both RGB and thermal images. Based on these descriptions, we propose the Multispectral Chain-of-Thought (MSCoT) prompting, which prompts the LLM to conduct reasoning steps and produce detections (Section IV-C). Detections from MSCoT prompting include single-modal (i.e., RGB and thermal) prediction scores S_{RGB}^L , S_T^L ,

and fused prediction scores S_F^L . In Sections IV-B and IV-C, we describe the processes to produce these detections in detail.

Language-driven Multi-modal Fusion (LMF). Vision-driven detection, language-driven detection, and vision-language fusion are performed to produce final detections, S_{LMF} and B_{LMF} . In Section IV-D, we describe the fusion strategies in detail.

B. Cross-modal Pedestrian Description Generation

The first step of the language branch is to generate text descriptions of pedestrians, both from the RGB and thermal images. We prompt a Multi-modal Large Language Model (MLLM) ChatGPT-4V [41] to describe pedestrian regions in the image, which can be identified by their bounding box coordinates B_{RGB} , B_T obtained from single-modal detectors. However, there are two challenges, which we introduce below with their solutions.

Detection Pairing. The first challenge is due to the misalignment in multispectral data [11], [15]. The same pedestrian often appears in different locations within the RGB and thermal image pairs, as their image sensors may have different Field-of-View or frame rates [15]. In such cases, we need to guide MLLMs to make descriptions based on different image regions in RGB and thermal images for the same pedestrians. Our strategy is to find the detection pairs from the single-modal detections (e.g., bounding boxes) that belong to the same pedestrians and provide this information to the MLLM.

Algorithm 1: Detection Pairing (DPair)

```

1: Input: Prediction scores  $S_{RGB}, S_T$ , Bounding boxes  $B_{RGB}, B_T$ .
2: Require: An IoU threshold  $\tau$ .
3: Output: Paired bounding boxes  $B^{paired}$ , paired prediction scores  $S^{paired}$ .
4:
5: procedure DPair( $B_{RGB}, B_T, S_{RGB}, S_T; \tau$ )
6:   initialize lists  $B \leftarrow B_{RGB} \cup B_T, S \leftarrow S_{RGB} \cup S_T,$ 
    $B^{paired} \leftarrow \phi,$  and  $S^{paired} \leftarrow \phi.$ 
7:   Find the box  $b_{max} \in B$  of the highest prediction score.
8:   Find boxes  $D \in B$  overlapping with  $b_{max}$ , of IoU ( $> \tau$ )
   in the opposite modality.
9:   Find the box  $b_{pair} \in D$  of the highest IoU value.
10:  If  $D$  is empty, then  $b_{pair} \leftarrow b_{max}$  and  $s_{pair} \leftarrow s_{max}.$ 
11:  Append  $(b_{max}, b_{pair})$  to  $B^{paired}.$ 
12:  Append  $(s_{max}, s_{pair})$  to  $S^{paired}.$ 
13:  Remove  $b_{max}$  and  $b_{pair}$  from  $B$  and  $s_{max}$  and  $s_{pair}$ 
   from  $S$ 
14:  Repeat this process until  $B$  and  $S$  are empty.
15:  return  $B^{paired}, S^{paired}$ 
16: end procedure

```

Algorithm 2: Visual Crop & Mark (VCM)

```

1: Input: An image  $X$ , and bounding boxes  $B$ .
2: Output: Pre-processed images  $X^{VCM}.$ 
3:
4: procedure VCM( $X, B$ )
5:   initialize  $X^{VCM} \leftarrow \phi.$ 
6:   for all bounding boxes  $b$  in  $B$ 
7:     Draw a green box at bounding box  $b$  in the
     image  $X.$ 
8:     Crop the image  $X$  around the bounding box  $b$ 
     such that the width and height of the cropped
     image  $X_c$  are twice as the width and height of  $b.$ 
9:     Append the cropped image  $X_c$  to  $X^{VCM}.$ 
10:  end for
11:  return  $X^{VCM}$ 
12: end procedure

```

Although bounding boxes representing the same pedestrian can have different coordinates in different modalities, still they will contain highly overlapping areas in the images, and those boxes will have large values of IoUs (Intersection-of-Unions). Specifically, for the i -th bounding box $b_{i,m}$ in bounding boxes B_m , obtained from the single-modal detector in the m modality (m is either RGB or thermal: T), we aim to find the bounding box from B_{m^c} , in the opposite modality m^c that corresponds to the same pedestrian. To this end, we compute the IoU value between $b_{i,m}$ across all bounding boxes in B_{m^c} , and find the box that has the highest IoU value, e.g., b_{j,m^c} , with $b_{i,m}$. Here, we only consider the boxes with IoU values above the IoU threshold τ . With indices i and j , we can find a pair of the prediction scores $s_{i,m}$ and s_{j,m^c} that belong to the same pedestrian. We call such tuples $(b_{i,m}, b_{j,m^c})$ and $(s_{i,m}, s_{j,m^c})$ as the ‘‘paired detection’’. When all IoU values are under the IoU threshold τ , this means that there are no boxes in B_{m^c} that correspond to the same pedestrian and $b_{i,m}$ can not find a pair. Such cases can occur at nighttime or in

thermal-obscured scenarios where the pedestrian is detected by only one modality. In this case, we override the value of $b_{i,m}$ and $s_{i,m}$ to the opposite modality, making pairs of $(b_{i,m}, b_{i,m})$ and $(s_{i,m}, s_{i,m})$. Iterating this process for over all bounding boxes in B_m and B_{m^c} (i.e., B_{RGB} and B_T) allows us to obtain a set of paired detections B^{paired} and S^{paired} . Denote the Detection Pairing Module as a function $DPair(\cdot)$ with respect to inputs B_{RGB}, B_T, S_{RGB} , and S_T , which indicate bounding boxes and prediction scores obtained from RGB and thermal single-modal detectors, respectively. The inputs and outputs of $DPair(\cdot)$ can be represented as:

$$S^{paired}, B^{paired} = DPair(B_{RGB}, B_T, S_{RGB}, S_T; \tau), \quad (4)$$

where τ indicates an IoU threshold. We set this value to 0.5, the standard value used in the object detection task. B^{paired} is used to guide MLLMs the location of when making descriptions in RGB and thermal images. S^{paired} is used when fusing prediction scores from vision and language branches in Section IV-D. The complete algorithm of the Detection Pairing Module is described in Algorithm 1.

Visual Crop & Mark (VCM). Another challenge when using MLLMs for making descriptions is the low accuracy of MLLMs on small-scale objects, i.e., objects occupying a small area in the image. To solve this issue, we refer to a recent method [76] that improves the performance of MLLMs on small visual details by pre-processing the input image with image cropping. Similarly, we zoom in on the target pedestrians and crop the image around it, such that visual information irrelevant to the pedestrian is removed. We find such a pre-processing strategy is shown to significantly improve the accuracy of MLLMs in describing small-scale pedestrians, near the level comparable to recognizing large-scale pedestrians.

The detailed algorithm for VCM is described in Algorithm 2. First, an image X and bounding boxes B are given as input. Note that B represents the locations of pedestrians in image X . For each bounding box b , the image X is cropped around b so that the width and height of the cropped image X_c are twice as b .

In addition to cropping, we visually guide the MLLM to describe a specific pedestrian by drawing a 1-pixel width ‘‘green’’ color (with RGB values (0,255,0)) box around a target pedestrian. We use the ‘‘green’’ color to draw the boxes because it is most distinctly in hue from human skin color, thus effective for distinguishing humans from the background. This process is iterated for all bounding boxes $b \in B$ for both a RGB image X_{RGB} and a thermal image X_T . Denote this the Visual Crop & Mark process as $VCM(\cdot)$, then the pre-processed RGB and thermal images X_{RGB}^{VCM} and X_T^{VCM} can be written as:

$$X_{RGB}^{VCM} \leftarrow VCM(X_{RGB}, B^{paired}), \quad (5)$$

$$X_T^{VCM} \leftarrow VCM(X_T, B^{paired}), \quad (6)$$

where X_{RGB} and X_T are RGB and thermal input images, and B^{paired} is the set of the paired bounding boxes. When pre-processing images in X_{RGB} and X_T , bounding boxes of the corresponding modality in B^{paired} are used only.

Algorithm 3: Cross-aligned Pedestrian Description Generation (CPDG)

```

1: Input: An RGB image  $X_{RGB}$ , an thermal image  $X_T$ ,
   prediction scores  $S_{RGB}$ ,  $S_T$  and bounding boxes  $B_{RGB}$ ,  $B_T$ .
2: Require: Input text prompts  $p_{RGB}$ ,  $p_T$ , and IoU threshold  $\tau$ .
   Detection pairing module  $DPair(\cdot)$ , Visual Crop & Mark
   module  $VCM(\cdot)$ . A pre-trained multimodal large language
   model  $MLLM(\cdot)$ .
3: Output: A set of RGB descriptions  $D_{RGB}$ , a set of thermal
   descriptions  $D_T$ , and paired detections  $S^{paired}$ ,  $B^{paired}$ .
4:
5: procedure CPDG( $X_{RGB}, X_T, S_{RGB}, S_T, B_{RGB}, B_T,$ 
    $p_{RGB}, p_T, \tau$ )
6:    $S^{paired}, B^{paired} \leftarrow DPair(B_{RGB}, B_T, S_{RGB}, S_T; \tau)$ .
7:    $X_{RGB}^{VCM} \leftarrow VCM(X_{RGB}, B^{paired})$ .
8:    $X_T^{VCM} \leftarrow VCM(X_T, B^{paired})$ .
9:   initialize list  $D_{RGB} \leftarrow \phi, D_T \leftarrow \phi$ .
10:  for all images  $x_{RGB}^{VCM}$  in  $X_{RGB}^{VCM}$ 
11:     $d_{RGB} = MLLM(x_{RGB}^{VCM}; p_{RGB})$ .
12:    Append the text description  $d_{RGB}$  to  $D_{RGB}$ .
13:  end for
14:  for all images  $x_T^{VCM}$  in  $X_T^{VCM}$ 
15:     $d_T = MLLM(x_T^{VCM}; p_T)$ .
16:    Append the text description  $d_T$  to  $D_T$ .
17:  end for
18:  return  $D_{RGB}, D_T, S^{paired}, B^{paired}$ .
19: end procedure

```

Generating Descriptions with MLLMs. For each pre-processed image $x_{RGB}^{VCM} \in X_{RGB}^{VCM}$ and $x_T^{VCM} \in X_T^{VCM}$, we prompt the MLLM as the following. For the RGB image, “*In this RGB image, what is in the green box?*” and for the thermal image, “*In this thermal image, what is in the green box?*”. Denote these prompts as p_{RGB} , and p_T . Then, we can generate their corresponding text descriptions d_{RGB} and d_T such as:

$$d_{RGB} \leftarrow MLLM(x_{RGB}^{VCM}; p_{RGB}), \quad (7)$$

$$d_T \leftarrow MLLM(x_T^{VCM}; p_T), \quad (8)$$

where $MLLM(\cdot)$ denotes the process of generating text descriptions from an MLLM, given the pre-processed image as input. Text descriptions are generated for all $x_{RGB}^{VCM} \in X_{RGB}^{VCM}$ and $x_T^{VCM} \in X_T^{VCM}$, producing sets of descriptions D_{RGB} and D_T . The detailed algorithm for Cross-modal Pedestrian Description Generation (CPDG) is described in Algorithm 3.

C. Multispectral Chain-of-Thought Prompting

In this section, we introduce Multispectral Chain-of-Thought (MSCoT) prompting, which facilitates LLMs to build step-by-step cross-modal rationales and produce detection results. MSCoT prompting first comprehends intra-modality information and produces single-modal prediction scores from each RGB and thermal description. Then, MSCoT prompting comprehends inter-modality reasoning and outputs fused detection scores and bounding boxes. This multi-step reasoning process addresses LLMs’ overconfidence [42] and produce calibrated confidence scores.

To this end, we refer to the Chain-of-Thought (CoT) prompting [46] technique, which significantly improves LLM’s reasoning ability in complex NLP tasks. CoTs add

a series of intermediate reasoning steps into LLMs and generate rationales when predicting answers. Motivated by the late-fusion process in multispectral pedestrian detection, we propose a Multispectral Chain-of-Thought (MSCoT) prompting chain. Given the text descriptions $d_{RGB} \in D_{RGB}$ and $d_T \in D_T$ of a RGB image and a thermal image, MSCoT prompting first prompts the LLM to produce single-modal prediction scores s_{RGB}^L , and s_T^L and then predict a fused prediction score s_F^L based on rationale chains. Given the descriptions d_{RGB} , and d_T of RGB and thermal images as the context, we design the following prompt chains:

Generating Single-modal Prediction.

Context: RGB image description d_{RGB} , thermal image description d_T .

Prompt: First, predict what is in the RGB image based on d_{RGB} . And predict what is in the thermal image based on d_T . Please answer in the format : [class, prediction score]

From the above prompt, the LLM outputs single-modal prediction scores s_{RGB}^L , and s_T^L . Additionally providing s_{RGB}^L , and s_T^L as the context, the following prompts for generating fused prediction scores and multispectral rationales are:

Generating Multispectral Rationales and Prediction.

Context: RGB image description: d_{RGB} , thermal image description: d_T , answers: s_{RGB}^L , and s_T^L .

Prompt: Based on the descriptions and your answers, predict what is in these aligned RGB and thermal images. Please answer in the format: [class, prediction score]

Then the LLM outputs fused prediction scores s_F^L . For all steps, the prediction scores s_{RGB}^L , s_T^L , and s_F^L are assigned only if the class outputs are “Person”. If not, the prediction scores are assigned as zero. s_{RGB}^L , s_T^L , and s_F^L can expressed as:

$$s_{RGB}^L, s_T^L, s_F^L = MSCoT(d_{RGB}, d_T). \quad (9)$$

Iterating this process over all $d_{RGB} \in D_{RGB}$ and $d_T \in D_T$ obtains the prediction scores: s_{RGB}^L , s_T^L , and s_F^L . Our implementation for MSCoT prompting is achieved by fine-tuning ChatGPT-3.5 [40] with about 50 training samples. The implementation details are described below.

Finetuning the LLM for MSCoT. We use the ChatGPT-3.5 (GPT-3.5) API [40], provided by the OpenAI developer platform. Using the fine-tuning module provided on the GPT official website [77], we trained GPT-3.5 API with our training data. The official document for GPT-3.5 [77] recommends training 50 samples for fine-tuning the model, and we utilized a total of 50 training samples for each FLIR and CVC-14 model. The training data contains textual descriptions of RGB and thermal images, rationale, and prediction scores for training the Large Language Model. We prompt the GPT-3.5 [40] consisting of rationale and prediction scores. The following answers are obtained by prompting the GPT-3.5 independently with these prompts, and we merge the answers to make the training data. Then with these data, we fine-

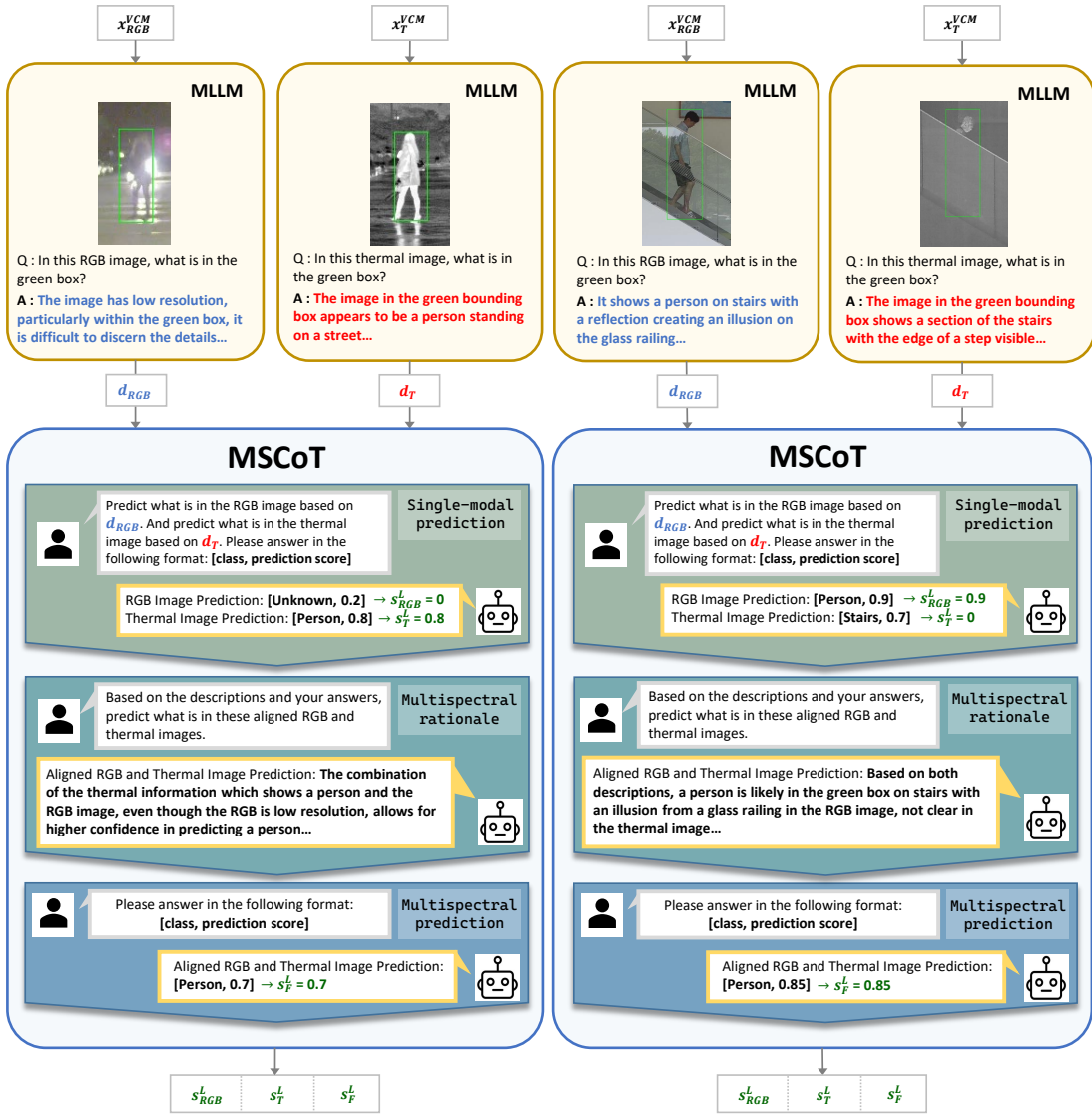


Fig. 5. Visualized process of our proposed Multispectral Chain-of-Thought (MSCoT) prompting.

tune the model answer based on a chain of prompts. The training data are manually selected with high-quality answers, containing reasonable rationales and confidence scores. 50 training data from the FLIR training images are used for fine-tuning the MSCoT of the FLIR model. Also, we made 50 training data using the CVC-14 training images for MSCoT of the CVC-14 model. Note that images from ROTX-MP are not used for making training data for MSCoT because it violates the evaluation setting for ROTX-MP.

D. Language-driven Multi-modal Fusion (LMF)

We propose to ensemble the detections of the vision branch and the language branch at the last stage of the proposed network (Fig. 3).

Vision-driven Detection. For the vision branch, denote S_{RGB}^V as the prediction scores from S^{paired} , and B_{RGB}^V as the bounding boxes from B^{paired} that corresponds to the RGB modality, similar for S_T^V and B_T^V . Then, the vision-driven

detections S_F^V (prediction scores) and B_F^V (bounding boxes) can be produced as:

$$S_F^V = \max(S_{RGB}^V, S_T^V), B_F^V = \frac{B_{RGB}^V \odot S_{RGB}^V + B_T^V \odot S_T^V}{S_{RGB}^V + S_T^V}, \quad (10)$$

where \odot denotes the Hadamard product (element-wise multiplication). NMS (Eq. 2) and weighted-averaging (Eq. 3) are applied for score-fusion and box-fusion.

Language-driven Detection. Next, for the language branch, fused bounding boxes B_F^L can be produced as:

$$B_F^L = \frac{B_{RGB}^L \odot S_{RGB}^L + B_T^L \odot S_T^L}{S_{RGB}^L + S_T^L}, \quad (11)$$

given the bounding boxes B_{RGB}^V, B_T^V obtained single-modal detectors. Weighted-averaging (Eq. 3) is applied for box-fusion. The fused prediction scores S_F^L are produced by the MSCoT prompting (Section IV-C).

Vision-Language Fusion. Lastly, final detections are pro-

duced as:

$$S_{LMF} = avg(S_F^V, S_F^L), B_{LMF} = \frac{S_F^V \odot B_F^V + S_F^L \odot B_F^L}{S_F^V + S_F^L}, \quad (12)$$

where S_{LMF} and B_{LMF} denote final prediction scores and bounding boxes. Averaging (Eq. 2) and weighted-averaging (Eq. 3) are applied for score-fusion and box-fusion.

Design Choice. For score-fusion, we adopted the NMS method (Eq. 2) in the vision-driven detection. NMS compares the prediction scores estimated in each modality and votes for the highest one, removing the lower score. We apply such a strategy because higher confidence scores generally occur when there is more useful information for detecting the pedestrian. From this strategy, we can obtain higher prediction scores for true-positive detections in most cases. However, it can also increase the prediction scores for false positives. As MSCoT prompting can comprehend very low prediction scores for false positives, we adopt the averaging strategy (Eq. 1) in the vision-language fusion to refine over-confident false positives from the vision-driven detections. For box-fusion, we adopted the weighting average (Eq. 3) method in all processes, implying that more confident detections should have a higher weight when fusing. In Section VII-B, we conduct an ablation study on these design choices.

V. EXPERIMENTAL SETUP

A. Dataset and Evaluation Metric

The experiments are conducted on multispectral pedestrian datasets: Teledyne FLIR Free ADAS Thermal Dataset v2.0.0 [30], CVC-14 [31], ROTX-MP [16]. The FLIR [30] dataset consists of RGB and thermal image pairs with an image resolution of 640×512 . For a fair comparison with previous studies [3], [16], [54], [78], we use the aligned version of FLIR, proposed by [78]. This version filters out misaligned images, containing well-aligned 4,129 training and 1,013 test RGB and thermal image pairs. For convenience, we call this version of the dataset as FLIR. Following previous works, we evaluate both day and night images and report the performance on the entire test set ('All'). In contrast to FLIR, the CVC-14 [31] dataset often contains heavily misaligned pairs of RGB and thermal images. The train and test set each contains 3,618 and 1,433 grayscale and thermal images with a 640×471 resolution. We evaluate daytime ('Day'), nighttime ('Night'), and the total ('All') test images separately, following previous works [15], [16].

Lastly, we evaluate our method on the ROTX-MP [16] dataset, which consists of 1,000 test images of mainly thermal-obscured pedestrians. We use the models trained from FLIR and CVC-14 to test on ROTX-MP, as this dataset aims to evaluate multispectral pedestrian detectors when there is a substantial distribution change between the train and test splits. For the evaluation metric, we use the Average Precision (AP \uparrow). These experimental settings are the same as the original paper [16].

B. Implementation Detail

Single-modal Detectors. For the single-modal detectors, we use the Co-DETR [79] model and train RGB images

and thermal images separately. Co-DETR is based on the DETR (DEtection TRansformer) [80] architecture, enhanced by collaborative learning with multiple parallel auxiliary heads integrated into the output of the transformer encoder. We train the single-modal detectors with RGB and thermal images from FLIR [30] and CVC-14 [31] training data, respectively. For optimizing Co-DETR, we use the same setting in the original paper [79], using AdamW [81] optimizer with an initial learning rate of $1e-4$ and weight decay of $1e-4$. All models are trained on an eight NVIDIA A6000 GPU for 16 epochs with a batch size of 16.

Large Language Models (LLMs). We use two types of Large Language Models. First is the Multimodal Large Language Model (MLLM), which we use to generate text descriptions for RGB and thermal pedestrian images (Section IV-B). For the MLLM, we use the pre-trained model of the ChatGPT-vision (GPT-4V) [41] API, provided by the OpenAI developer platform.

The second is the chatbot version, ChatGPT-3.5 (GPT-3.5) API [40], also provided by the OpenAI developer platform. We fine-tuned the GPT-3.5 model for the Multispectral Chain-of-Thought (MSCoT) prompting (Section IV-C) we proposed. Using the fine-tuning module provided on the GPT official website [77], we trained GPT-3.5 API with our high-quality selection pairs consisting of RGB, thermal descriptions, rationale, and prediction scores. The official document for GPT-3.5 [77] recommends training 50 samples for fine-tuning the model, and we utilized a total of 50 training samples.

C. Comparison Model

We compare our method with five multispectral pedestrian detection models: 1) Halfway Fusion [5], 2) Cross-modality Fusion Transformer (CFT) [54], 3) Kim et al. [15], 4) ProbEn [18], and 5) Causal Mode Multiplexer (CMM) [16]. We used the same experimental settings as their original papers. **Halfway Fusion:** we use the Faster-RCNN [82] as the base model and train the model for 3 epochs. The learning rate is initialized at 0.008 during the initial 2 epochs with SGD and subsequently applied a 0.1 learning rate decay for the final epoch. **CFT:** The initial learning rate is 0.01 with a momentum of 0.937, and weight decay 0.0005. Batch size is 32 and the model is trained for 200 epochs and the YOLO-v5 weight trained on the COCO dataset is used for weight initialization. We used the official code. **Kim et al:** The learning rate is initialized at 0.006 during the initial 2 epochs and a 0.1 learning rate decay was applied for the final epoch. We used the official code. **ProbEn:** We finetune two single-modal detectors based on Faster R-CNN [82] pretrained on COCO [83]. The Detectron 2 [84] library is used. We used SGD [85] optimizer with learning rate $5e-3$. We adopt the 'ProbEn' score fusion and 'v-avg' box fusion because such combinations are shown the most effective in the original paper [18]. Also, we adopt the E+M+T ensemble version, indicating that early-fusion, mid-fusion, and thermal single-modal detectors are ensembles. **CMM** [16]: The CMM framework is based on the Uncertainty-guided model [15], with the FPN architecture with ResNet-50 [86]. The learning

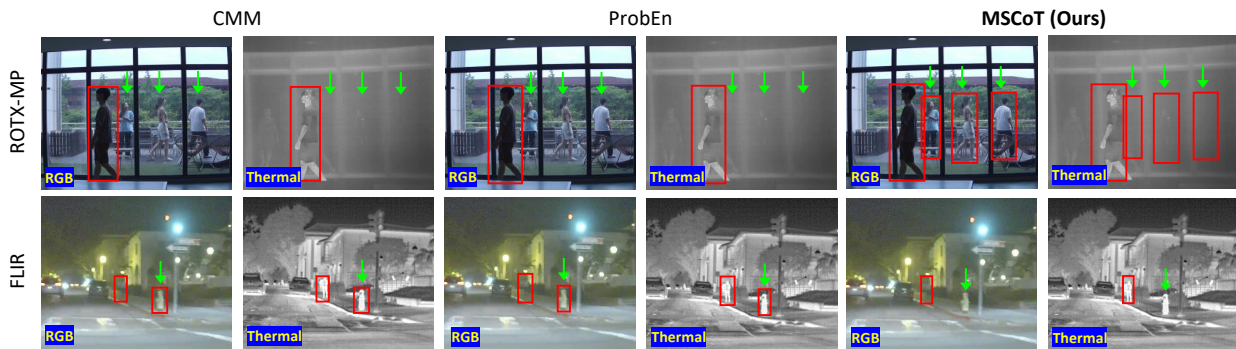


Fig. 6. Visualized detections on the ROTX-MP [16] (Top) and FLIR [30] (Bottom) datasets. (Top): MSCoTDet can detect pedestrians over the window (\downarrow), in which their thermal signatures are absent due to the window. In contrast, other models (CMM [16], ProbEn [18]) fail to detect these pedestrians. (Bottom): Moreover, other models create false-positive detections on the fireplug (\downarrow) due to its thermal signature similar-looking to pedestrians. In contrast, MSCoTDet (Ours) makes correct predictions.

Train	FLIR	CVC-14		Modality Used		
Test	FLIR	CVC-14				
Metric	AP (\uparrow)	MR (\downarrow)		RGB	Thermal	Language
Method	All	Day	Night	All		
Halfway Fusion [5]	75.85	36.29	26.29	31.99	✓	✓
CFT [54]	84.10	18.81	25.25	21.83	✓	✓
Kim et al. [15]	84.67	23.87	11.08	18.7	✓	✓
CMM [16]	87.8	27.81	7.71	17.13	✓	✓
ProbEn [18]	86.74	23.01	21.02	22.23	✓	✓
MSCoTDet (Ours)	90.39	6.69	13.69	10.39	✓	✓

Train	FLIR	CVC-14		Modality Used		
Test	ROTX-MP	ROTX-MP				
Metric	AP (\uparrow)	AP (\uparrow)		RGB	Thermal	Language
Method	All	All				
Halfway Fusion [5]	36.95	8.8		✓	✓	
CFT [54]	3.64	8.58		✓	✓	
Kim et al. [15]	21.69	13.36		✓	✓	
CMM [16]	57.09	34.96		✓	✓	
ProbEn [18]	17.2	16.66		✓	✓	
MSCoTDet (Ours)	67.33	57.65		✓	✓	✓

TABLE I

DETECTION PERFORMANCE ON THE FLIR [30], CVC-14 [31] (LEFT), AND ROTX-MP [16] (RIGHT). (LEFT): WE TRAIN AND TEST ON FLIR, CVC-14 DATASETS. (RIGHT): WE TRAIN MODELS ON FLIR, CVC-14, AND EVALUATE MODELS ON THE ROTX-MP DATASET. WE ADOPT THIS EXPERIMENTAL SETTING FOLLOWING THE ORIGINAL PAPER [16] TO EVALUATE MODELS WHEN THERE IS A SIGNIFICANT DISTRIBUTION DIFFERENCE BETWEEN TRAIN AND TEST SETS. WE COMPARE OUR PROPOSED METHOD WITH DIFFERENT MULTISPECTRAL PEDESTRIAN DETECTION MODELS [5], [15], [16], [18], [54] RECENTLY PROPOSED. THE BEST RESULTS ARE HIGHLIGHTED.

rate is initialized at 0.007 during the initial 1 epoch and then a 0.1 learning rate decay is applied for the final epoch. The Region of Interests (RoIs) per image is set to $N=300$. We apply switchable Total Indirect Effect (sTIE) for every ROI and compute the prediction score. We used the official code, with the same settings as the original paper [16].

VI. EXPERIMENTAL RESULT

A. Result on FLIR, and CVC-14

We train and test on FLIR [30], CVC-14 [31] datasets to evaluate whether our method performs well on general multispectral pedestrian data. We report the detection performance of different models on these datasets. For the evaluation metrics, we follow existing studies on multispectral pedestrian detection to measure the detection performances on these datasets and make a fair comparison. Specifically, we use average precision (AP) on FLIR ('All'). For CVC-14, we use the log-average miss rate (MR) for evaluating models and report the performance on daytime ('Day') and nighttime ('Night'), and the entire set ('All') of images separately. Note that lower MR (MR \downarrow) and higher AP (AP \uparrow) values indicate better detection performance.

Table I (Left) shows the experimental results on the FLIR and CVC-14 test set. On FLIR ('All'), MSCoTDet achieves the highest AP (90.39 AP), which surpasses other methods

by at least 2.59 AP. Such results indicate the effectiveness of MSCoTDet on well-aligned data. On CVC-14, MSCoTDet demonstrates the lowest miss rate among models in ('Day'), and ('All'), with a value of 6.69 MR and 10.39 MR, respectively. Our method surpasses other models by at least 12.12 MR for ('Day') and 6.74 MR for ('All'). As ('All') indicates the entire dataset, our method achieves the best performance also on CVC-14. Such results illustrate that MSCoTDet is also effective on a dataset that largely contains misaligned multispectral data.

B. Result on ROTX-MP

Experimenting with models on the ROTX-MP [16] dataset is to evaluate modality bias and their generalizability when there is a significant distributional change in test data. Following the original work [16], we train models on general datasets (FLIR [30], and CVC-14 [31]) and test models on ROTX-MP. The results are in Table I (Right). MSCoTDet achieves the best performance on ROTX-MP for both cases when trained on FLIR and CVC-14. When trained from FLIR, MSCoTDet achieves the highest AP (67.33 AP), which outperforms other methods by at least 10.24 AP. When trained from CVC-14, MSCoTDet achieves the highest AP (57.65 AP), which outperforms other methods by at least 22.69 AP. Such results indicate that MSCoTDet has a better ability to intervene in modality bias compared to other models.

Train	FLIR	CVC-14				Modality Used		
Test	FLIR	CVC-14						
Metric	AP (\uparrow)	MR (\downarrow)						
Method	All	Day	Night	All	RGB	Thermal	Language	
RGB only	76.06	31.55	40.10	36.07	✓			
Thermal only	85.73	43.24	33.44	36.07		✓		
Late-fusion	88.60	18.33	18.86	21.57	✓	✓		
MSCoTDet (Ours)	90.39	6.69	13.69	10.39	✓	✓	✓	

Train	FLIR	CVC-14		Modality Used		
Test	ROTX-MP	ROTX-MP				
Metric	AP (\uparrow)	AP (\uparrow)				
Method	All	All	All	RGB	Thermal	Language
RGB only	54.20	31.05		✓		
Thermal only	19.33	9.10			✓	
Late-fusion	58.95	44.72		✓	✓	
MSCoTDet (Ours)	67.33	57.65		✓	✓	✓

TABLE II

ABLATION STUDY ON THE EFFECT OF USING LANGUAGE MODELS. OUR FOCUS IS TO COMPARE MSCoTDet WITH ‘LATE-FUSION’, THE VISION BRANCH EQUIPPED WITH VISION-DRIVEN DETECTION OF MSCoTDet.

Train		FLIR		CVC-14		
Test		FLIR		CVC-14		
Method		AP (\uparrow)		MR (\downarrow)		
V	VL	All	Day	Night	All	All
Avg	Avg	89.47	10.98	17.38	16.12	
Avg	Max	88.31	10.26	18.53	15.71	
Max	Max	89.94	8.83	17.54	14.07	
Max	Avg	90.39	6.69	13.69	10.39	

Train		FLIR		CVC-14	
Test		ROTX-MP		ROTX-MP	
Method		AP (\uparrow)		AP (\uparrow)	
V	VL	All	All	All	All
Avg	Avg	66.22	56.69		
Avg	Max	66.27	56.60		
Max	Max	66.31	56.02		
Max	Avg	67.33	57.65		

TABLE III

ABLATION STUDY ON THE SCORE-FUSION STRATEGY. WE COMPARE THE 1) AVG, AVG, 2) AVG, MAX, 3) MAX, MAX, AND 4) MAX, AVG STRATEGIES IN THE VISION-DRIVEN DETECTION (‘V’) AND IN THE VISION-LANGUAGE FUSION (‘VL’).

VII. ABLATION STUDY

A. Effect of Integrating Language Models

We conduct an ablation study to evaluate the effectiveness of integrating large language models to our framework. As our framework fuses detection results from both the vision branch and the language branch, one might ask: *how much does the language branch boost overall performance?* For the ablation study, we compare MSCoTDet and three detection models: (1) ‘RGB only’, (2) ‘Thermal only’, and (3) ‘Late-fusion’. First, the ‘RGB only’, and the ‘Thermal only’ model indicate single-modal detection in the vision branch of MSCoTDet. Second, ‘Late-fusion’ is in which the single-modal detections of ‘RGB only’ and ‘Thermal only’ are fused, i.e., equivalent to the vision branch equipped with vision-driven detection of our framework. Thus, to measure the effect of using large language models, our main focus is to compare ‘Late-fusion’ with MSCoTDet. The results are shown in Table II. Our method achieves higher performance than ‘Late-fusion’ in all FLIR [30], CVC-14 [31], and ROTX-MP [16]. The results on the FLIR and CVC-14 indicate that integrating large language models can improve the overall performance of multispectral pedestrian detectors in general datasets. Also, the results on ROTX-MP indicate that using language models can significantly improve the generalizability of multispectral pedestrian detectors, and effectively mitigate the modality bias.

B. Effect of the Fusion Strategy

We conduct an ablation study to evaluate the design choice of our fusion strategy in Section IV-D. Our fusion strategies include score-fusion and box-fusion. For score-fusion, we adopt the Non-maximum Suppression (NMS) in the vision-driven detection (‘V’) and averaging strategy in the vision-language

Train		FLIR		CVC-14			
Test		FLIR		CVC-14			
Method		AP (\uparrow)		MR (\downarrow)			
V	L	VL	All	Day	Night	All	All
argmax	argmax	argmax	89.49	7.56	17.64	14.00	
s-avg	argmax	argmax	89.79	8.03	15.28	12.63	
argmax	s-avg	argmax	89.83	8.32	15.39	13.31	
s-avg	s-avg	argmax	90.32	7.60	15.14	12.54	
argmax	argmax	s-avg	89.49	6.25	18.51	14.18	
s-avg	argmax	s-avg	90.32	7.63	15.19	11.99	
argmax	s-avg	s-avg	89.73	6.85	16.81	13.47	
s-avg	s-avg	s-avg	90.39	6.69	13.69	10.39	

Train		FLIR		CVC-14	
Test		ROTX-MP		ROTX-MP	
Method		AP (\uparrow)		AP (\uparrow)	
V	L	VL	All	All	All
argmax	argmax	argmax	66.10	56.97	
s-avg	argmax	argmax	66.29	56.95	
argmax	s-avg	argmax	67.03	56.90	
s-avg	s-avg	argmax	67.24	57.13	
argmax	argmax	s-avg	66.11	57.01	
s-avg	argmax	s-avg	67.28	56.99	
argmax	s-avg	s-avg	67.15	57.21	
s-avg	s-avg	s-avg	67.33	57.65	

TABLE IV

ABLATION STUDY ON THE BOX-FUSION STRATEGY. WE EXPERIMENT ARGMAX AND S-AVG FOR EACH VISION-DRIVEN DETECTION (‘V’), LANGUAGE-DRIVEN DETECTION (‘L’), AND VISION-LANGUAGE FUSION (‘VL’).

fusion (‘VL’), respectively. NMS compares the prediction scores estimated in each modality and votes for the highest one, removing the lower scores (Eq. 2). The averaging strategy averages prediction scores estimated in each modality (Eq. 1). Denote the averaging strategy as ‘Avg’ and NMS as ‘Max’. For the comparison study, we conducted experiments on the (1) Avg, Avg, (2) Avg, Max, and (3) Max, Max fusion strategies in each vision-driven detection (‘V’) and vision-language fusion (‘VL’), respectively. We do not compare different score-fusion in the language branch, as we use our proposed method: MSCoT (Section IV-C) produces prediction scores from fused modalities. All other conditions are kept the same. The results are shown in Table III. The Max, Avg strategy consistently performs the best in all test sets.

For box-fusion, we adopt weighted averaging (Eq. 3) for all vision-driven detection (‘V’), language-driven detection (‘L’), and vision-language fusion (‘VL’). Denote the weighted averaging strategy as ‘s-avg’. For the comparison study, we consider the NMS box fusion, denoted as ‘argmax’, and compare between a total of 8 combinations (either s-avg or max in three parts). All other conditions are kept the same as our MSCoTDet design during all experiments. The results are shown in Table IV. Applying s-avg for all V, L, and VL shows the best performance for most test cases.

VIII. CONCLUSION

In this paper, we introduced MSCoTDet, a novel framework integrating Multispectral Chain-of-Thought (MSCoT) prompting strategy with traditional vision-based multispectral pedestrian detection. By leveraging the generalization capabilities of Large Language Models (LLMs), MSCoTDet

effectively addresses modality bias and enhances detection accuracy in multispectral pedestrian detection tasks without additional data supervision. To this end, we design the Language-driven Multi-modal Fusion (LMF) to enable fusion between the detection results obtained from MSCoT and vision-based multispectral pedestrian detectors. Our extensive experiments demonstrated that MSCoTDet outperforms existing methods on standard datasets such as FLIR and CVC-14, achieving significant improvements in Average Precision (AP) and Miss Rates. Furthermore, MSCoTDet achieved impressive performance on the ROTX-MP dataset, proving the generalizability even when substantial distribution differences exist between training and testing data.

REFERENCES

- [1] Yiming Sun, Bing Cao, Pengfei Zhu, and Qinghua Hu, "Drone-based rgb-infrared cross-modality vehicle detection via uncertainty-aware learning," *IEEE Transactions on Circuits and Systems for Video Technology*, vol. 32, no. 10, pp. 6700–6713, 2022.
- [2] Dayan Guan, Yanpeng Cao, Jiangxin Yang, Yanlong Cao, and Michael Ying Yang, "Fusion of multispectral data through illumination-aware deep neural networks for pedestrian detection," *Information Fusion*, vol. 50, pp. 148–157, 2019.
- [3] Taeheon Kim, Youngjoon Yu, and Yong Man Ro, "Multispectral invisible coating: laminated visible-thermal physical attack against multispectral object detectors using transparent low-e films," in *Proceedings of the AAAI Conference on Artificial Intelligence*, 2023, vol. 37, pp. 1151–1159.
- [4] Dan Xu, Wanli Ouyang, Elisa Ricci, Xiaogang Wang, and Nicu Sebe, "Learning cross-modal deep representations for robust pedestrian detection," in *Proceedings of the IEEE conference on computer vision and pattern recognition*, 2017, pp. 5363–5371.
- [5] Jingjing Liu, Shaoting Zhang, Shu Wang, and Dimitris N Metaxas, "Multispectral deep neural networks for pedestrian detection," *arXiv preprint arXiv:1611.02644*, 2016.
- [6] Chengyang Li, Dan Song, Ruofeng Tong, and Min Tang, "Illumination-aware faster r-cnn for robust multispectral pedestrian detection," *Pattern Recognition*, vol. 85, pp. 161–171, 2019.
- [7] Lu Zhang, Zhiyong Liu, Shifeng Zhang, Xu Yang, Hong Qiao, Kaizhu Huang, and Amir Hussain, "Cross-modality interactive attention network for multispectral pedestrian detection," *Information Fusion*, vol. 50, pp. 20–29, 2019.
- [8] Lu Zhang, Xiangyu Zhu, Xiangyu Chen, Xu Yang, Zhen Lei, and Zhiyong Liu, "Weakly aligned cross-modal learning for multispectral pedestrian detection," in *Proceedings of the IEEE/CVF international conference on computer vision*, 2019, pp. 5127–5137.
- [9] Taeheon Kim, Hong Joo Lee, and Yong Man Ro, "Map: Multispectral adversarial patch to attack person detection," in *ICASSP 2022-2022 IEEE International Conference on Acoustics, Speech and Signal Processing (ICASSP)*. IEEE, 2022, pp. 4853–4857.
- [10] Jung Uk Kim, Sungjune Park, and Yong Man Ro, "Uncertainty-guided cross-modal learning for robust multispectral pedestrian detection," *IEEE Transactions on Circuits and Systems for Video Technology*, vol. 32, no. 3, pp. 1510–1523, 2021.
- [11] Soonmin Hwang, Jaesik Park, Namil Kim, Yukyung Choi, and In So Kweon, "Multispectral pedestrian detection: Benchmark dataset and baseline," in *Proceedings of the IEEE conference on computer vision and pattern recognition*, 2015, pp. 1037–1045.
- [12] Kailai Zhou, Linsen Chen, and Xun Cao, "Improving multispectral pedestrian detection by addressing modality imbalance problems," in *Computer Vision—ECCV 2020: 16th European Conference, Glasgow, UK, August 23–28, 2020, Proceedings, Part XVIII 16*. Springer, 2020, pp. 787–803.
- [13] Qing Li, Changqing Zhang, Qinghua Hu, Pengfei Zhu, Huazhu Fu, and Lei Chen, "Stabilizing multispectral pedestrian detection with evidential hybrid fusion," *IEEE Transactions on Circuits and Systems for Video Technology*, 2023.
- [14] Jörg Wagner, Volker Fischer, Michael Herman, Sven Behnke, et al., "Multispectral pedestrian detection using deep fusion convolutional neural networks," in *ESANN*, 2016, vol. 587, pp. 509–514.
- [15] Jung Uk Kim, Sungjune Park, and Yong Man Ro, "Uncertainty-guided cross-modal learning for robust multispectral pedestrian detection," *IEEE Transactions on Circuits and Systems for Video Technology*, vol. 32, no. 3, pp. 1510–1523, 2022.
- [16] Taeheon Kim, Sebin Shin, Youngjoon Yu, Hak Gu Kim, and Yong Man Ro, "Causal mode multiplexer: A novel framework for unbiased multispectral pedestrian detection," 2024.
- [17] Fang Qingyun, Han Dapeng, and Wang Zhaokui, "Cross-modality fusion transformer for multispectral object detection," 2022.
- [18] Yi-Ting Chen, Jinghao Shi, Zelin Ye, Christoph Mertz, Deva Ramanan, and Shu Kong, "Multimodal object detection via probabilistic ensembling," in *European Conference on Computer Vision*. Springer, 2022, pp. 139–158.
- [19] Taeheon Kim, Youngjoon Yu, and Yong Man Ro, "Defending physical adversarial attack on object detection via adversarial patch-feature energy," in *Proceedings of the 30th ACM International Conference on Multimedia*, 2022, pp. 1905–1913.
- [20] Piotr Dollar, Christian Wojek, Bernt Schiele, and Pietro Perona, "Pedestrian detection: An evaluation of the state of the art," *IEEE transactions on pattern analysis and machine intelligence*, vol. 34, no. 4, pp. 743–761, 2011.
- [21] Wei-Yen Hsu and Wen-Yen Lin, "Ratio-and-scale-aware yolo for pedestrian detection," *IEEE transactions on image processing*, vol. 30, pp. 934–947, 2020.
- [22] Irtiza Hasan, Shengcai Liao, Jinpeng Li, Saad Ullah Akram, and Ling Shao, "Generalizable pedestrian detection: The elephant in the room," in *Proceedings of the IEEE/CVF Conference on Computer Vision and Pattern Recognition*, 2021, pp. 11328–11337.
- [23] Xinwen Fan, Yukang Zhang, Yang Lu, and Hanzi Wang, "Parformer: transformer-based multi-task network for pedestrian attribute recognition," *IEEE Transactions on Circuits and Systems for Video Technology*, 2023.
- [24] Sungjune Park, Hyunjun Kim, and Yong Man Ro, "Integrating language-derived appearance elements with visual cues in pedestrian detection," *IEEE Transactions on Circuits and Systems for Video Technology*, 2024.
- [25] Yi Shi, Shixuan Zhao, Jiang Wu, Zhangbi Wu, and Hongmei Yan, "Fixated object detection based on saliency prior in traffic scenes," *IEEE Transactions on Circuits and Systems for Video Technology*, 2023.
- [26] Muhammad Bilal, Asim Khan, Muhammad Umar Karim Khan, and Chong-Min Kyung, "A low-complexity pedestrian detection framework for smart video surveillance systems," *IEEE Transactions on Circuits and Systems for Video Technology*, vol. 27, no. 10, pp. 2260–2273, 2016.
- [27] Mira Jeong, Byoung Chul Ko, and Jae-Yeal Nam, "Early detection of sudden pedestrian crossing for safe driving during summer nights," *IEEE transactions on circuits and systems for video technology*, vol. 27, no. 6, pp. 1368–1380, 2016.
- [28] Xiaoyu Chen, Hongliang Li, Qingbo Wu, King Ngi Ngan, and Linfeng Xu, "High-quality r-cnn object detection using multi-path detection calibration network," *IEEE Transactions on Circuits and Systems for Video Technology*, vol. 31, no. 2, pp. 715–727, 2020.
- [29] Jung Uk Kim, Jungsu Kwon, Hak Gu Kim, and Yong Man Ro, "Bbc net: Bounding-box critic network for occlusion-robust object detection," *IEEE transactions on circuits and systems for video technology*, vol. 30, no. 4, pp. 1037–1050, 2019.
- [30] Inc FLIR Systems, "Free teledyne flir thermal dataset for algorithm training," <https://www.flir.com/oem/adas/adas-dataset-form/>, 2021, Accessed: 2022-08-05.
- [31] Alejandro González, Zhijie Fang, Yainuvis Socarras, Joan Serrat, David Vázquez, Jiaolong Xu, and Antonio M López, "Pedestrian detection at day/night time with visible and fir cameras: A comparison," *Sensors*, vol. 16, no. 6, pp. 820, 2016.
- [32] Yulei Niu, Kaihua Tang, Hanwang Zhang, Zhiwu Lu, Xian-Sheng Hua, and Ji-Rong Wen, "Counterfactual vqa: A cause-effect look at language bias," in *Proceedings of the IEEE/CVF Conference on Computer Vision and Pattern Recognition*, 2021, pp. 12700–12710.
- [33] Long Ouyang, Jeffrey Wu, Xu Jiang, Diogo Almeida, Carroll Wainwright, Pamela Mishkin, Chong Zhang, Sandhini Agarwal, Katarina Slama, Alex Ray, et al., "Training language models to follow instructions with human feedback," *Advances in Neural Information Processing Systems*, vol. 35, pp. 27730–27744, 2022.
- [34] Tom Brown, Benjamin Mann, Nick Ryder, Melanie Subbiah, Jared D Kaplan, Prafulla Dhariwal, Arvind Neelakantan, Pranav Shyam, Girish Sastry, Amanda Askell, et al., "Language models are few-shot learners," *Advances in neural information processing systems*, vol. 33, pp. 1877–1901, 2020.
- [35] BigScience Workshop, Teven Le Scao, Angela Fan, Christopher Akiki, Ellie Pavlick, Suzana Ilić, Daniel Hesslow, Roman Castagné, Alexandra Sasha Luccioni, François Yvon, et al., "Bloom: A 176b-parameter open-access multilingual language model," *arXiv preprint arXiv:2211.05100*, 2022.
- [36] Hugo Touvron, Thibaut Lavril, Gautier Izacard, Xavier Martinet, Marie-Anne Lachaux, Timothée Lacroix, Baptiste Rozière, Naman Goyal, Eric Hambro, Faisal Azhar, et al., "Llama: Open and efficient foundation language models," *arXiv preprint arXiv:2302.13971*, 2023.
- [37] Aakanksha Chowdhery, Sharan Narang, Jacob Devlin, Maarten Bosma, Gaurav Mishra, Adam Roberts, Paul Barham, Hyung Won Chung,

- Charles Sutton, Sebastian Gehrmann, et al., "Palm: Scaling language modeling with pathways," *Journal of Machine Learning Research*, vol. 24, no. 240, pp. 1–113, 2023.
- [38] Jordan Hoffmann, Sebastian Borgeaud, Arthur Mensch, Elena Buchatskaya, Trevor Cai, Eliza Rutherford, Diego de Las Casas, Lisa Anne Hendricks, Johannes Welbl, Aidan Clark, et al., "Training compute-optimal large language models," *arXiv preprint arXiv:2203.15556*, 2022.
- [39] Zhuosheng Zhang, Aston Zhang, Mu Li, Hai Zhao, George Karypis, and Alex Smola, "Multimodal chain-of-thought reasoning in language models," *arXiv preprint arXiv:2302.00923*, 2023.
- [40] Inc OpenAI, "Chatgpt-3.5 turbo api," <https://chat.openai.com/>, 2023, Accessed: 2024-02-29.
- [41] Josh Achiam, Steven Adler, Sandhini Agarwal, Lama Ahmad, Ilge Akkaya, Florencia Leoni Aleman, Diogo Almeida, Janko Altmenschmidt, Sam Altman, Shyamal Anadkat, et al., "Gpt-4 technical report," *arXiv preprint arXiv:2303.08774*, 2023.
- [42] Miao Xiong, Zhiyuan Hu, Xinyang Lu, Yifei Li, Jie Fu, Junxian He, and Bryan Hooi, "Can llms express their uncertainty? an empirical evaluation of confidence elicitation in llms," *arXiv preprint arXiv:2306.13063*, 2023.
- [43] Moxin Li, Wenjie Wang, Fuli Feng, Fengbin Zhu, Qifan Wang, and Tat-Seng Chua, "Think twice before assure: Confidence estimation for large language models through reflection on multiple answers," *arXiv preprint arXiv:2403.09972*, 2024.
- [44] Gianluca Detommaso, Martin Bertran, Riccardo Fogliato, and Aaron Roth, "Multicalibration for confidence scoring in llms," *arXiv preprint arXiv:2404.04689*, 2024.
- [45] Gwenth Portillo Wightman, Alexandra DeLucia, and Mark Dredze, "Strength in numbers: Estimating confidence of large language models by prompt agreement," in *Proceedings of the 3rd Workshop on Trustworthy Natural Language Processing (TrustNLP 2023)*, 2023, pp. 326–362.
- [46] Jason Wei, Xuezhi Wang, Dale Schuurmans, Maarten Bosma, Fei Xia, Ed Chi, Quoc V Le, Denny Zhou, et al., "Chain-of-thought prompting elicits reasoning in large language models," *Advances in Neural Information Processing Systems*, vol. 35, pp. 24824–24837, 2022.
- [47] Jiale Cao, Yanwei Pang, Shengjie Zhao, and Xuelong Li, "High-level semantic networks for multi-scale object detection," *IEEE Transactions on Circuits and Systems for Video Technology*, vol. 30, no. 10, pp. 3372–3386, 2019.
- [48] Jung Uk Kim, Seong Tae Kim, Hong Joo Lee, Sangmin Lee, and Yong Man Ro, "Cua loss: Class uncertainty-aware gradient modulation for robust object detection," *IEEE Transactions on Circuits and Systems for Video Technology*, vol. 31, no. 9, pp. 3529–3543, 2020.
- [49] Shifeng Zhang, Longyin Wen, Zhen Lei, and Stan Z Li, "Refinedet++: Single-shot refinement neural network for object detection," *IEEE Transactions on Circuits and Systems for Video Technology*, vol. 31, no. 2, pp. 674–687, 2020.
- [50] Wanli Ouyang, Xingyu Zeng, and Xiaogang Wang, "Partial occlusion handling in pedestrian detection with a deep model," *IEEE Transactions on Circuits and Systems for Video Technology*, vol. 26, no. 11, pp. 2123–2137, 2015.
- [51] Yifan Jiao, Hantao Yao, and Changsheng Xu, "Pen: Pose-embedding network for pedestrian detection," *IEEE Transactions on Circuits and Systems for Video Technology*, vol. 31, no. 3, pp. 1150–1162, 2020.
- [52] Sungjune Park, Hyunjun Kim, and Yong Man Ro, "Robust pedestrian detection via constructing versatile pedestrian knowledge bank," *Pattern Recognition*, p. 110539, 2024.
- [53] Youngjoon Yu, Hong Joo Lee, Hakmin Lee, and Yong Man Ro, "Defending person detection against adversarial patch attack by using universal defensive frame," *IEEE Transactions on Image Processing*, vol. 31, pp. 6976–6990, 2022.
- [54] Fang Qingyun, Han Dapeng, and Wang Zhaokui, "Cross-modality fusion transformer for multispectral object detection," *arXiv preprint arXiv:2111.00273*, 2021.
- [55] Chengyang Li, Dan Song, Ruofeng Tong, and Min Tang, "Multispectral pedestrian detection via simultaneous detection and segmentation," *arXiv preprint arXiv:1808.04818*, 2018.
- [56] Weiyao Wang, Du Tran, and Matt Feiszli, "What makes training multi-modal classification networks hard?," in *Proceedings of the IEEE/CVF conference on computer vision and pattern recognition*, 2020, pp. 12695–12705.
- [57] Xulin Li, Yan Lu, Bin Liu, Yating Liu, Guojun Yin, Qi Chu, Jinyang Huang, Feng Zhu, Rui Zhao, and Nenghai Yu, "Counterfactual intervention feature transfer for visible-infrared person re-identification," in *European conference on computer vision*. Springer, 2022, pp. 381–398.
- [58] Ehsan Abbasnejad, Damien Teney, Amin Parvaneh, Javen Shi, and Anton van den Hengel, "Counterfactual vision and language learning," in *Proceedings of the IEEE/CVF conference on computer vision and pattern recognition*, 2020, pp. 10044–10054.
- [59] Zujie Liang, Weitao Jiang, Haifeng Hu, and Jiaying Zhu, "Learning to contrast the counterfactual samples for robust visual question answering," in *Proceedings of the 2020 conference on empirical methods in natural language processing (EMNLP)*, 2020, pp. 3285–3292.
- [60] Tejas Gokhale, Pratyay Banerjee, Chitta Baral, and Yezhou Yang, "Mutant: A training paradigm for out-of-distribution generalization in visual question answering," *arXiv preprint arXiv:2009.08566*, 2020.
- [61] Long Chen, Xin Yan, Jun Xiao, Hanwang Zhang, Shiliang Pu, and Yueting Zhuang, "Counterfactual samples synthesizing for robust visual question answering," in *Proceedings of the IEEE/CVF conference on computer vision and pattern recognition*, 2020, pp. 10800–10809.
- [62] Aishwarya Agrawal, Dhruv Batra, Devi Parikh, and Aniruddha Kembhavi, "Don't just assume; look and answer: Overcoming priors for visual question answering," in *Proceedings of the IEEE conference on computer vision and pattern recognition*, 2018, pp. 4971–4980.
- [63] Itai Gat, Idan Schwartz, Alexander Schwing, and Tamir Hazan, "Removing bias in multi-modal classifiers: Regularization by maximizing functional entropies," *Advances in Neural Information Processing Systems*, vol. 33, pp. 3197–3208, 2020.
- [64] Yue Yang, Artemis Panagopoulou, Shenghao Zhou, Daniel Jin, Chris Callison-Burch, and Mark Yatskar, "Language in a bottle: Language model guided concept bottlenecks for interpretable image classification," in *Proceedings of the IEEE/CVF Conference on Computer Vision and Pattern Recognition*, 2023, pp. 19187–19197.
- [65] Muhammad Ferjad Naeem, Muhammad Gul Zain Ali Khan, Yongqin Xian, Muhammad Zeshan Afzal, Didier Stricker, Luc Van Gool, and Federico Tombari, "I2mvformer: Large language model generated multi-view document supervision for zero-shot image classification," in *Proceedings of the IEEE/CVF Conference on Computer Vision and Pattern Recognition*, 2023, pp. 15169–15179.
- [66] Zaid Khan, Vijay Kumar BG, Samuel Schuster, Xiang Yu, Yun Fu, and Manmohan Chandraker, "Q: How to specialize large vision-language models to data-scarce vqa tasks? a: Self-train on unlabeled images!," in *Proceedings of the IEEE/CVF Conference on Computer Vision and Pattern Recognition*, 2023, pp. 15005–15015.
- [67] Cees GM Snoek, Marcel Worring, and Arnold WM Smeulders, "Early versus late fusion in semantic video analysis," in *Proceedings of the 13th annual ACM international conference on Multimedia*, 2005, pp. 399–402.
- [68] Georgios Tzifas and Hamidreza Kasaei, "Early or late fusion matters: Efficient rgb-d fusion in vision transformers for 3d object recognition," in *2023 IEEE/RSJ International Conference on Intelligent Robots and Systems (IROS)*. IEEE, 2023, pp. 9558–9565.
- [69] Tri Minh Nguyen, Thin Nguyen, Thao Minh Le, and Truyen Tran, "Gefa: early fusion approach in drug-target affinity prediction," *IEEE/ACM transactions on computational biology and bioinformatics*, vol. 19, no. 2, pp. 718–728, 2021.
- [70] Chen Chen, Ruizhe Li, Yuchen Hu, Sabato Marco Siniscalchi, Pin-Yu Chen, Ensiong Chng, and Chao-Han Huck Yang, "It's never too late: Fusing acoustic information into large language models for automatic speech recognition," *arXiv preprint arXiv:2402.05457*, 2024.
- [71] Emilie Morvant, Amaury Habrard, and Stéphane Ayache, "Majority vote of diverse classifiers for late fusion," in *Structural, Syntactic, and Statistical Pattern Recognition: Joint IAPR International Workshop, S+ SSPR 2014, Joensuu, Finland, August 20-22, 2014. Proceedings*. Springer, 2014, pp. 153–162.
- [72] Ekaterina Shutova, Douwe Kiela, and Jean Maillard, "Black holes and white rabbits: Metaphor identification with visual features," in *Proceedings of the 2016 conference of the North American chapter of the association for computational linguistics: Human language technologies*, 2016, pp. 160–170.
- [73] Yiqun Yao and Rada Mihalcea, "Modality-specific learning rates for effective multimodal additive late-fusion," in *Findings of the Association for Computational Linguistics: ACL 2022*, 2022, pp. 1824–1834.
- [74] Jack Hessel and Lillian Lee, "Does my multimodal model learn cross-modal interactions? it's harder to tell than you might think!," *arXiv preprint arXiv:2010.06572*, 2020.
- [75] Yagya Raj Pandeya and Joonwhoan Lee, "Deep learning-based late fusion of multimodal information for emotion classification of music video," *Multimedia Tools and Applications*, vol. 80, pp. 2887–2905, 2021.
- [76] Jiarui Zhang, Mahyar Khayatkhoei, Prateek Chhikara, and Filip Ilievski, "Visual cropping improves zero-shot question answering of multimodal large language models," *arXiv preprint arXiv:2310.16033*, 2023.
- [77] Inc OpenAI, "Gpt-3.5 turbo fine-tuning and api updates," <https://openai.com/blog/gpt-3-5-turbo-fine-tuning-and-api-updates>, 2023, Accessed: 2024-02-29.
- [78] Heng Zhang, Elisa Fromont, Sébastien Lefevre, and Bruno Avignon, "Multispectral fusion for object detection with cyclic fuse-and-refine blocks," in *2020 IEEE International conference on image processing (ICIP)*. IEEE, 2020, pp. 276–280.

- [79] Zhuofan Zong, Guanglu Song, and Yu Liu, “Detrs with collaborative hybrid assignments training,” in *Proceedings of the IEEE/CVF international conference on computer vision*, 2023, pp. 6748–6758.
- [80] Nicolas Carion, Francisco Massa, Gabriel Synnaeve, Nicolas Usunier, Alexander Kirillov, and Sergey Zagoruyko, “End-to-end object detection with transformers,” 2020.
- [81] Ilya Loshchilov and Frank Hutter, “Decoupled weight decay regularization,” *arXiv preprint arXiv:1711.05101*, 2017.
- [82] Ross Girshick, “Fast r-cnn,” in *Proceedings of the IEEE international conference on computer vision*, 2015, pp. 1440–1448.
- [83] Tsung-Yi Lin, Michael Maire, Serge Belongie, James Hays, Pietro Perona, Deva Ramanan, Piotr Dollár, and C Lawrence Zitnick, “Microsoft coco: Common objects in context,” in *Computer Vision—ECCV 2014: 13th European Conference, Zurich, Switzerland, September 6–12, 2014, Proceedings, Part V 13*. Springer, 2014, pp. 740–755.
- [84] Yuxin Wu, Alexander Kirillov, Francisco Massa, Wan-Yen Lo, and Ross Girshick, “Detectron2,” <https://github.com/facebookresearch/detectron2>, 2019.
- [85] Shun-ichi Amari, “Backpropagation and stochastic gradient descent method,” *Neurocomputing*, vol. 5, no. 4-5, pp. 185–196, 1993.
- [86] Kaiming He, Xiangyu Zhang, Shaoqing Ren, and Jian Sun, “Deep residual learning for image recognition,” in *Proceedings of the IEEE conference on computer vision and pattern recognition*, 2016, pp. 770–778.